Proceedings World Geothermal Congress 2015
Melbourne, Australia, 19-25 April 2015

Identifying Optimal Conditions for Sustainable Heat Production in Enhanced Geothermal Reservoirs Using Numerical Sensitivity Studies

Riahi, A. and Damjanac, B.

Itasca Consulting Group, Minneapolis, Minnesota 55401, United States

ariahi@itascacg.com, branko@itascacg.com

Keywords: Discrete element modeling, discrete fracture network, thermo-hydro-mechanically coupled processes, enhanced geothermal systems

ABSTRACT

This study is focused on a series of sensitivity studies with respect to series of key field and operational parameters in Enhanced Geothermal Reservoirs (EGS) and postulates the optimal conditions for heat extraction. The conclusions are drawn based on a series of numerical sensitivity studies that evaluate response of EGS during both stimulation and heat production phases. Two-dimensional models of reservoirs with explicit representation of the pre-existing discrete fracture network are simulated using the discrete element technique. A series of metrics including shear-stimulated area, injectivity, produced water temperature and produced power are evaluated for each case. Comparison of these metrics provides insight into the effect and range of importance of these parameters, and leads to identifying the optimal in-situ and operational condition.

1. INTRODUCTION

It is widely accepted that the response of Enhanced Geothermal Systems (EGS) is greatly affected by the pre-existing discrete fracture network. However, due to the complex thermo-hydromechanical response of these systems, predicting the response has proven to be a challenge. The objective of this study is to evaluate the sensitivity of sustainable heat production in EGS to various in-situ and operational parameters, and to identify the factors that affect production the most.

The numerical modeling approach is based on the discrete element technique in which the pre-existing discrete fracture network is generated stochastically and explicitly represented. In the adopted technique, the transient laminar flow through the pre-existing fracture network is simulated. The advective heat transfer by fluid flow, the convection at the boundary between moving fluid and rock, and the conduction of heat through surrounding rock are taken into account (for more details , refer to Riahi et al., 2014). The thermal response of the model is first verified against available solutions (Gringarten et al., 1975). The mechanical solution is fully coupled with thermal and hydraulic responses.

Using thermo-hydromechanically coupled numerical modeling approach, it is studied how field conditions (e.g., fracture size distribution, fracture spacing, fracture dilatational angle) and operational parameters (e.g., production rate) and well positioning affect the response of EGS during stimulation and production. In particular, the effect of well position with respect to orientation of fractures, distance between injection and production wells, and also slight variation in the location of wells are studied.

The numerical model set-up and assumptions, and the case studies are presented in Section 2. For each study, the correlation between heat production metrics and in-situ characteristics and operation parameters is studied by evaluating injectivity, productivity and generated thermal energy. Also, it is studied how stimulation can improve or degrade production.

2. NUMERICAL MODEL OF LARGE-SCALE RESERVOIRS AND RESULTS

2.1 Model Set-up

In all study cases presented in this paper, a horizontal section of a typical 2-km by 2-km enhanced geothermal reservoir at a depth of 2500 m is modelled. The pre-existing Discrete Fracture Network (DFN) is represented explicitly in this study. Definition, characteristics and the procedure for creation and simplification of DFN are presented in Riahi and Damjanac (2013a and 2013b). The fracture length distribution follows a power law distribution, which relates the probability of the occurrence of a fracture with a length of l to the negative exponent of the length, i.e., $n(l) \propto l^{-a}$. Also, it is assumed that all DFNs are fully connected, i.e., all fractures are interconnected and the connected cluster of fractures extends to the boundaries of the model.

It is assumed that the DFN consists of two fracture sets. Both the primary and secondary fracture sets are oriented favorably (at angles of 160° and 45° with respect to the major principal stress) for slip. The pressure required for shearing on these fractures is below the hydraulic fracturing pressure (i.e., smaller than the minor principal stress). The primary set is defined as the fracture set that requires a lower pressure for slip. It is assumed that the pre-existing fractures are already open and conductive, with the same initial apertures of all fractures within each fracture set. The primary and secondary fracture sets are assigned initial apertures of 3×10^{-5} m and 1×10^{-5} m, respectively. It is attempted that the reservoirs match an initial permeability close to 1×10^{-18} m^2. The failure criterion of the pre-existing fractures is defined by the Coulomb slip law with zero cohesion, a friction angle of 30° and dilation angle of 7.5°.

The numerical analyses are carried out using a discrete-element modeling approach using numerical code *Universal Distinct Element Code, UDEC,* (Itasca, 2011). The rock formation is represented by an assembly of rock blocks separated by a pre-existing fracture network. Fluid flow can occur only within the fractures. The blocks are considered to be impermeable and elastic. The pre-existing fractures are represented explicitly, as discontinuities that deform elastically, but also can open and slip (as governed by the Coulomb slip law) as a function of pressure and total stress.

In this study, propagation of pre-existing fractures is not considered. In order to model propagation of a hydraulic fracture (HF), the trajectory of the fracture is defined explicitly in the model before starting the analysis. The HF is assumed to be planar, aligned with the direction of the major principal stress. The two "incipient surfaces" of the HF plane are bonded initially with a strength that is equivalent to a specified fracture toughness. Propagation of the HF corresponds to breaking of these bonds.

In each of the cases presented, both the stimulation and production phases are modeled. The purpose of the stimulation phase is to increase permeability of the rock mass by injecting fluid into the reservoir at pressures sufficient to cause dilational slip on joints. The rate used during stimulation in the two-dimensional model (representative of unit thickness of the reservoir) is 2×10^{-4} $m^3/s/m$, which is equal to 0.07 m^3/s or 70 kg/s for the assumed reservoir thickness of 350 m. Typically, the stimulation phase is carried out for 120 hours. Only coupled hydromechanical processes are simulated during the stimulation phase; thermal effects are not included (i.e., considered not significant for the duration of the stimulation phase). The results of the stimulation phase, after excess pressures are dissipated, are used as initial conditions for the production phase.

Subsequent to the stimulation phase, the pressures are allowed to dissipate to the hydrostatic state before the production phase starts. The injection rate used during production is 1.5×10^{-4} $m^3/s/m$ (except the case stud on the effect of production rate). It is assumed that the reservoir has a temperature of 200°C, and the injected cold water temperature is 25°C. During the production phase, which is simulated for typical periods of five to 10 years, the thermal effects are important and a different solution method is used. A flow model is coupled with models of heat transported by advection and conduction, and the mechanical model of rock deformation. Thermo-hydromechanical interactions are represented because (1) the fluid flow is a strong function of the fracture aperture, (2) the fracture aperture is a function of temperature and mechanical deformation, (3) stresses in rock are influenced by temperature change and (4) changes in fluid flow affect how heat is distributed in the rock. For further reading on the assumption and implementation of the thermal solution coupled with hydromechanical solution refer to Riahi et al. (2014). For each case study, production indices such as temperature of the produced water, injection pressure, produced power and injectivity (i.e., injection rate divided by the pressure) are assessed.

Figure 1 shows the geometry and set-up of the *UDEC* model. The model represents a two-dimensional horizontal section through a reservoir with an assumed thickness of 350 m. It is assumed that the injection is through a vertical well that is located at the center of the model. The core part of the model containing the DFN is embedded into a larger domain with a regular network of pipes with a permeability equivalent to that of the core region. The linear dimensions of the full model are almost twice as large as those of the core part. The state of stress in the plane of the model is assumed to be anisotropic with the maximum principal horizontal stress equal to the vertical stress and the minimum principal horizontal stress equal to half of the vertical stress.

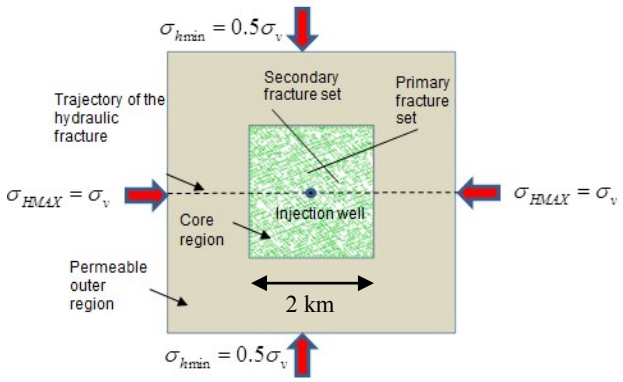

Figure 1: Geometry and model set-up.

2.2 Study 1: Effect of well positioning

For this study, a single production-well configuration is considered. A reservoir with a given DFN realization is stimulated for 120 hours, and subsequently nine different scenarios for location of the production well are considered. The DFN model used in this study has an exponent, α equal to 2; however the fracture size is capped to 300 m.

Contours of permanent aperture increase and locations of production wells are shown in Figure 2. The wells are located 250 m, 500 m and 800 m from the injection well. Also, three different cases with respect to the orientation of fractures are considered:

(a) *Case I:* the production well located (relative to the position of the injection well) in the direction of the primary fracture;

(b) *Case II:* the production well located in the direction of the secondary fracture; and

(c) *Case III:* the production well located between the two directions.

The nine scenarios are shown in Figure 2. Considering the change of apertures in the stimulated reservoir, the location of the wells in most cases is chosen such that they are positioned within the stimulated region. It is also studied how production is affected when the production well is located outside of the stimulated rock volume.

Out of the nine considered scenarios, *Cases I* and *II* for 800-m well spacing did not result in a substantial recovery of injected fluid. In *Case I*, the production well is located outside the stimulated region. In *Case II*, the well is located within the stimulated region; however, the flow takes a different, least resistant path as shown in Figure 3.

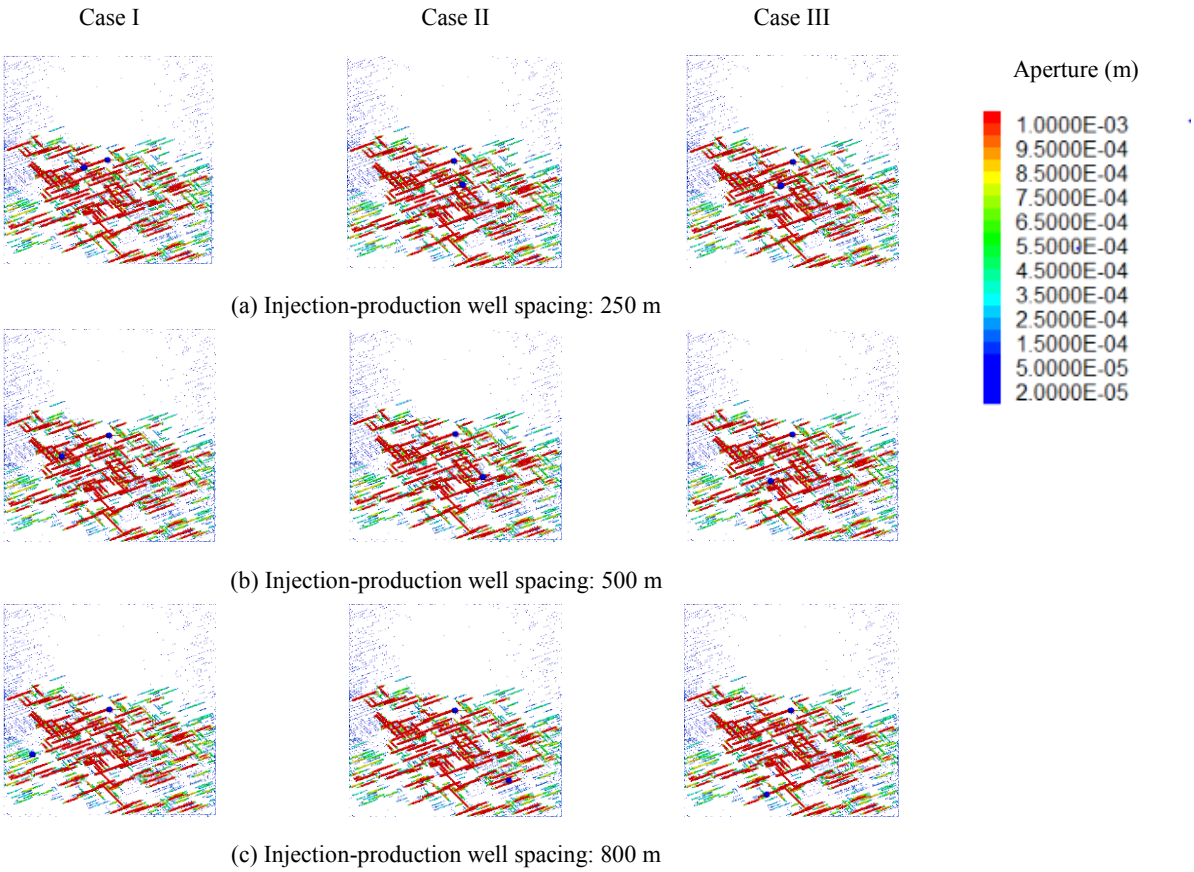

(a) Injection-production well spacing: 250 m

(b) Injection-production well spacing: 500 m

(c) Injection-production well spacing: 800 m

Figure 2. Effect of well positioning: Nine scenarios for a production well location.

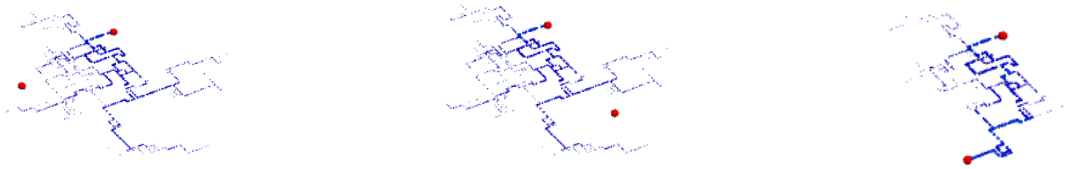

Case I Case II Case III

Figure 3. Effect of well positioning: Flow path for cases I, II and III with a well spacing of 800 m.

Figure 4 shows production indices for this study. Figure 4 (a) and (b) show that for all well distances considered, the produced water temperature in Case I has the quickest draw-down, while the injection pressure is the lowest. However, again considering all well distances, it seems that Case II and III have resulted in the better produced power. Figure 5 shows the rock temperature contours. From this figure, it can be interpreted that for well distances of 250 m and 500 m, Case I has resulted in the shortest flow path, which is the reason for lower required injection pressure. At the same time, the short flow path also has led to quickest temperature drawdown. From this figure, it also seems that Case II exhibits a more tortuous and longer flow path, which provides a greater heat exchange surface, and thus, results in slower temperature decay. However, this is achieved at a cost of higher pressure and lower injectivity.

For each case of injection-production well spacing, the average produced thermal power and injectivity for the three well orientation scenarios (i.e., case I, II and III) are shown in Figure 6. The average produced power represents average of the generated power for the three cases over a five-year period, while the average injectivity represents the average between three scenarios for the first year of production.

Overall, *Case III* with a well spacing of 800 m shows the highest produced power, which is the direct result of the longest flow path. However, the trade-off in this case is greater uncertainty of recovery of the injected fluid, as seen for *Cases I* and *II* with a well spacing of 800 m.

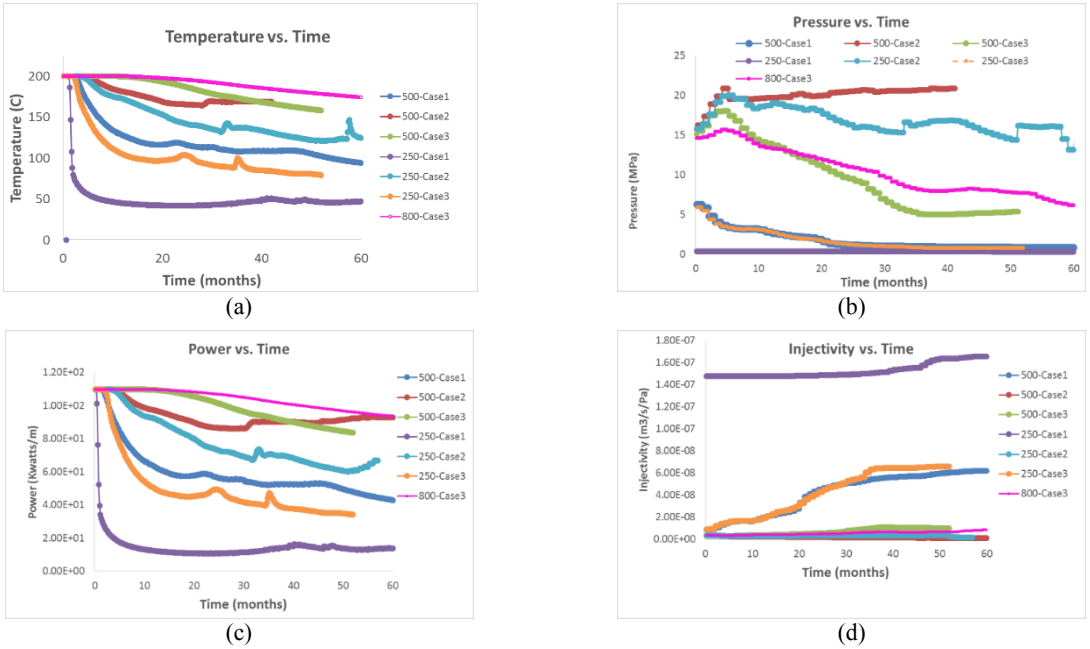

Figure 4. Effect of well positioning: Production indices for different well-production locations.

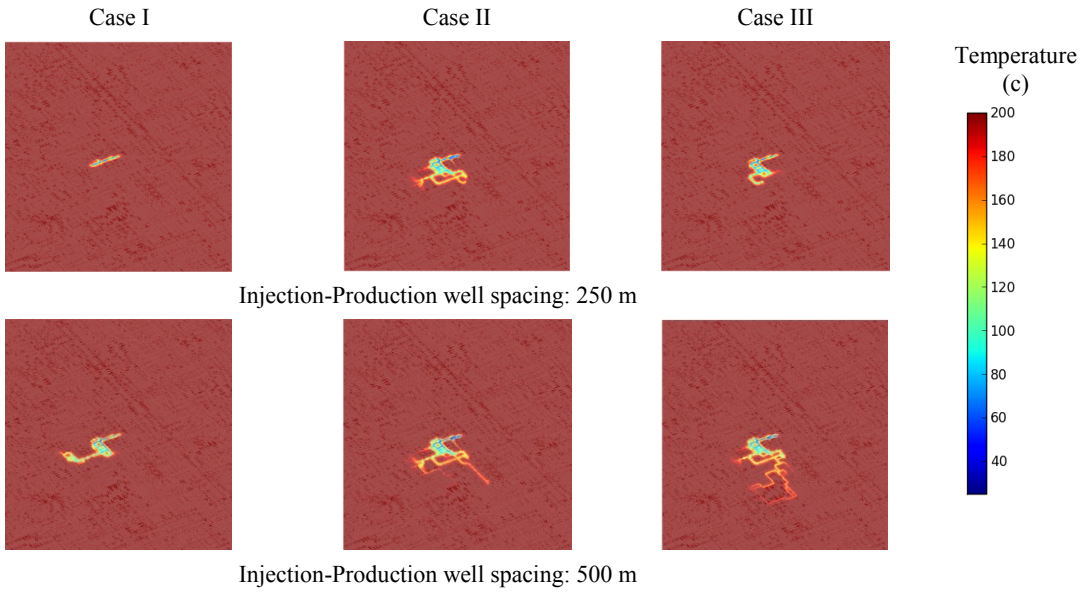

Figure 5. Effect of well positioning: Contours of rock temperature after 32 months of production; well spacing of (a) 250 m and (b) 500 m.

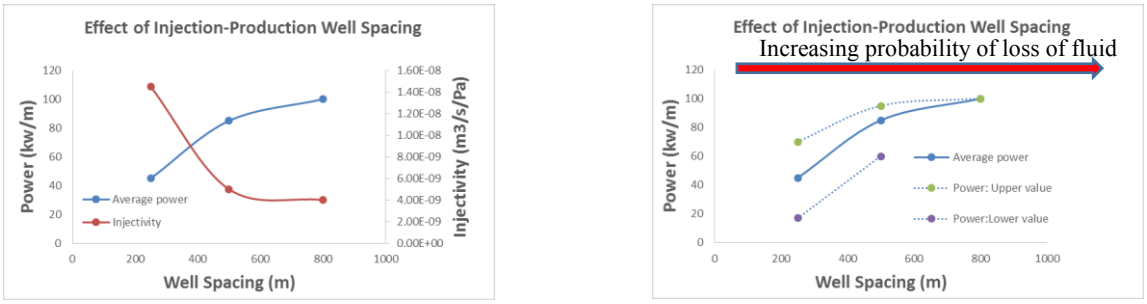

Figure 6. Effect of well positioning: Average generated thermal power and injectivity for injection-production well spacing. Averaging is for three well orientation scenarios. Thermal power represents average over five-year production, while injectivity represents average over the first year.

2.3 Study 2: Effect of fracture spacing

This study is focused on the effect of average fracture spacing in enhanced geothermal reservoirs. Three average spacing of 30 m, 55 m and 80 m are enforced for fractures. The DFN model used in this study has an exponent, α equal to 2, however the fracture size is capped to 300 m. The model with the average spacing of 30 m is considered the base case that approximately matches the specified permeability of 1 $\times 10^{-18}$ m^2. Clearly, as the spacing increases the density of fractures, and also the permeability of the reservoirs decrease. However, in all cases, it is enforced that the fracture network remains fully connected.

Figure 7 shows the stimulated indices with different fracture spacing after 120 hours of stimulation. As expected, the area of affected fractures and also shear stimulated area decreases with increasing spacing. Also, Figure 7 shows that as spacing increases, the potential of hydraulic fracturing increases, as seen for the case for spacing of 800 m. Figure 8 shows stimulated fracture region and location of production wells.

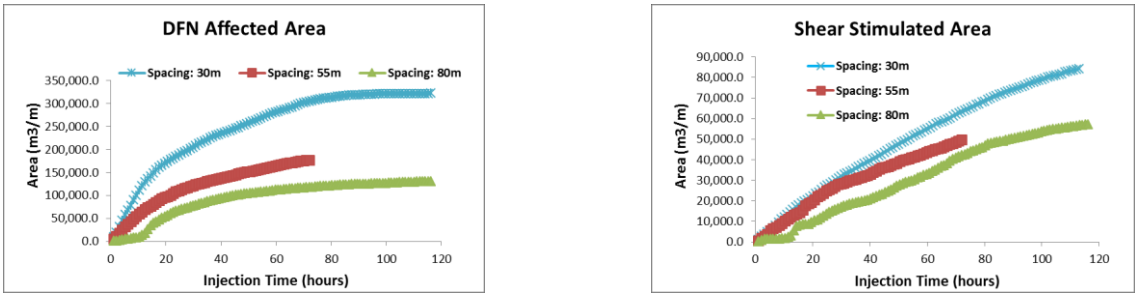

(a) DFN affected area

(b) Shear stimulated area

Figure 7. Effect of fracture spacing: Stimulation indices for different fracture spacing.

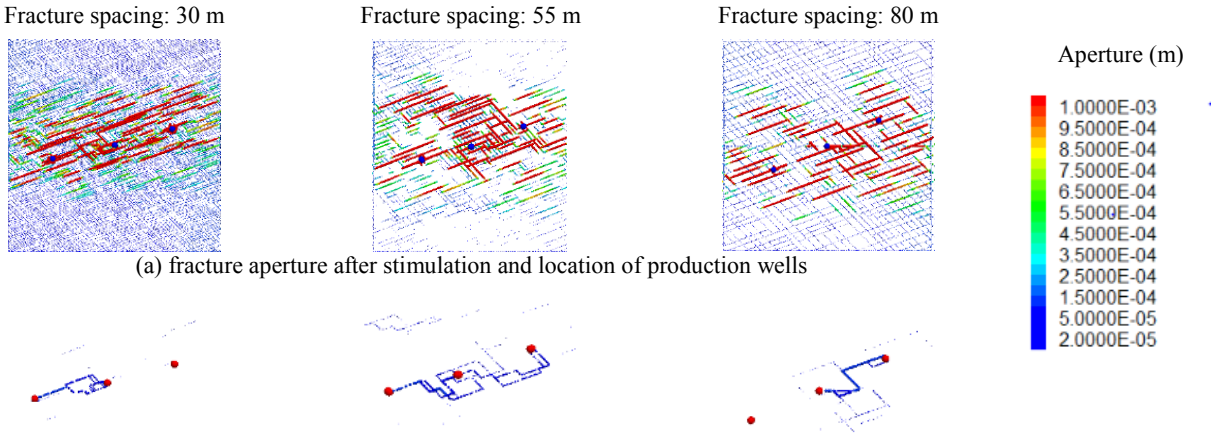

(a) fracture aperture after stimulation and location of production wells

(b) flow path

Figure 8. Effect of fracture spacing: Stimulation region, well positioning and flow path for models with fracture spacing.

Figure 9 and Figure 13 show the production indices for the case study on fracture spacing with two different injection-production well spacing of 500 m and 700 m. For the case of 500 m well spacing (Figure 9) the recovery rate for all three models with different fracture spacing is close to 100%. However, as shown in Figure 8, in the model with spacing of 55 m, both wells have become producing, which resulted in lower produced rate at each well, and thus, slower average temperature draw-down and higher generated power. Comparing the average generated power in model with fracture spacing of 30 to that of the model with fracture spacing of 80 m, an average 20% improvement in generated power is observed for the cases with well spacing of 500 m (shown in Figure 10). The variation in injectivity does not follow a monotonic response, which can be due to occurrence of hydraulic fracture in the model with fracture spacing of 800 m, and other localized aspects around the injection well. However, overall it is expected that the model with closest fracture spacing shows better injectivity due to higher permeability.

Comparing production indices for the cases with well spacing of 700 (Figure 13) shows that the trend of temperature draw down and power are not only affected by fracture spacing, but also with recovered rate. In the case of 700-m spacing, a couple of well positions are studied for each model. As the spacing increases, the potential of leak-off also increases. Figure 11 shows the rock temperature draw down in these models. In some of these models (30-m spacing Case I and 55-m spacing Case I), both wells have become producing while in others (30-m spacing Case II and 80-m scraping Case II), only one well is predicting with a recovery rate more than 90%. The model with fracture spacing of 80-case II resulted in a very low recovery of almost 55%, and thus the results could not be directly compared to the rest of the examples. Direct comparison could only be made between the models with 30-m spacing Case I and 55-m spacing Case I, which had a similar produced rate from one well, and indicate a 15-20% improvement for cases with closer fracture spacing. Average generated power for all these cases is presented in Figure 12.

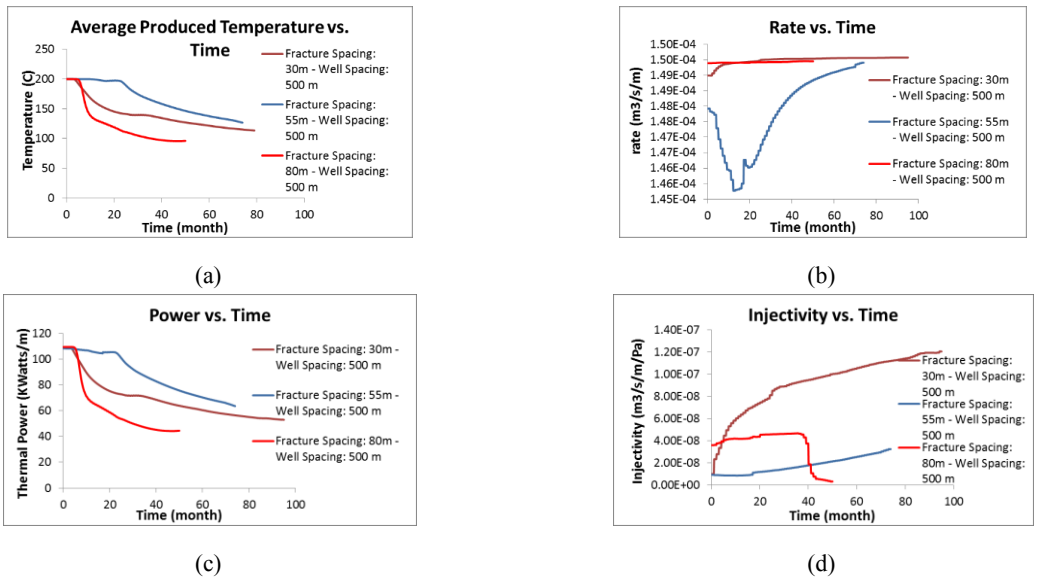

Figure 9. Effect of fracture spacing: Production indices for different fracture spacing and well spacing of 500 m.

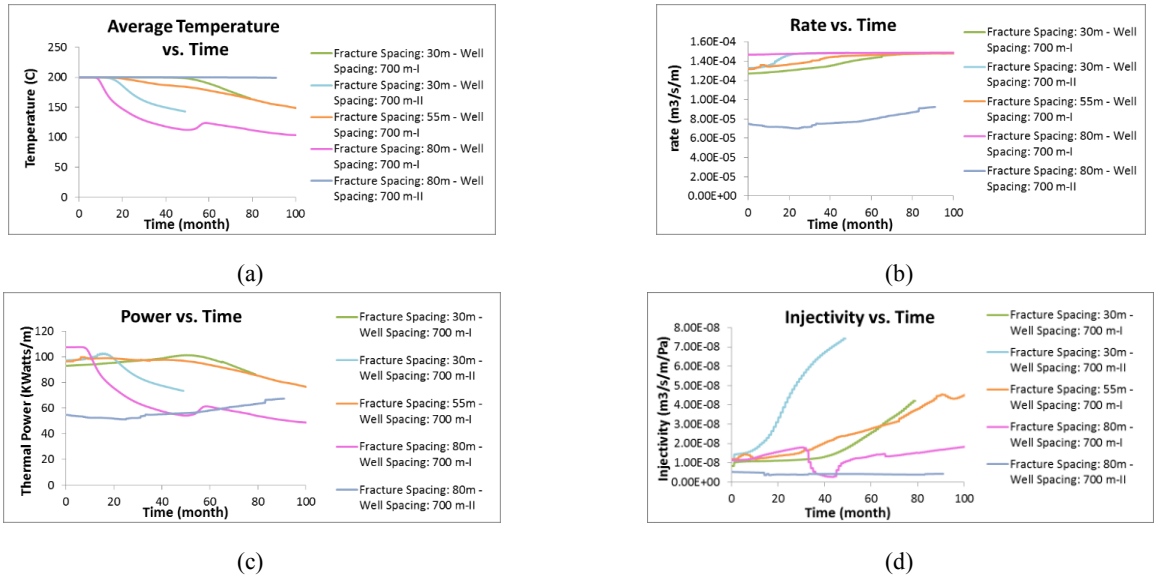

Figure 10. Effect of fracture spacing: Production indices for different fracture spacing and well spacing of 700 m.

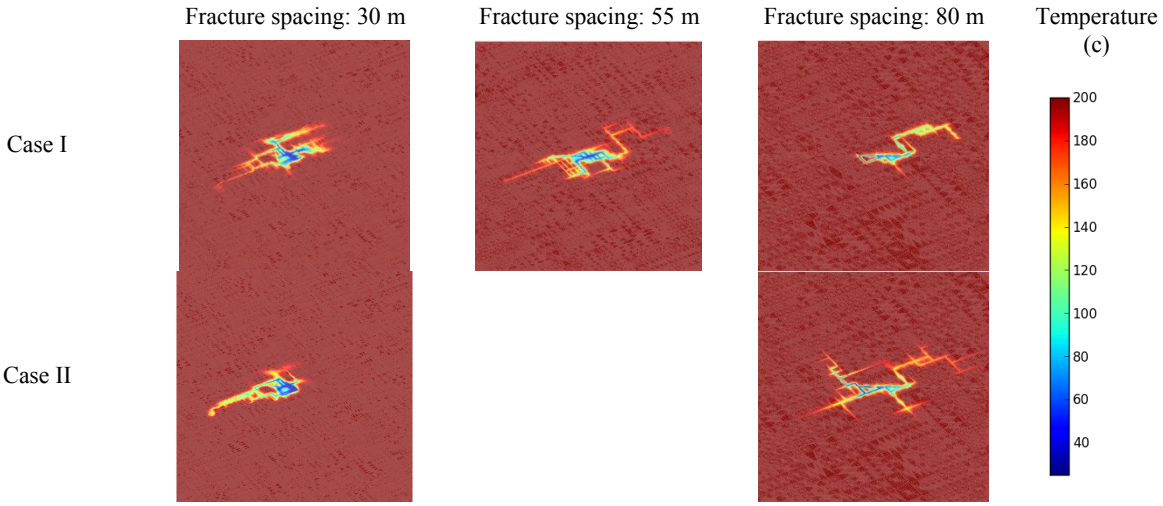

Figure 11. Effect of fracture spacing: Rock temperature draw-down after 60 months.

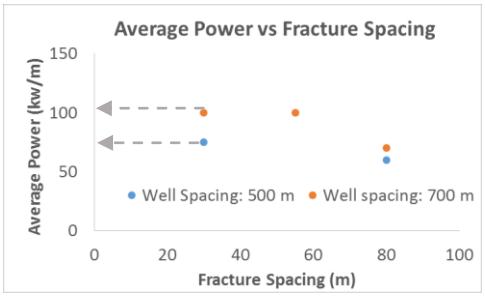

Figure 12. Effect of fracture spacing: Average generated power over a period of five years.

2.4 Study 3: Effect of dilation angle

This case study investigates the effect of fracture dilation angle. As indicated in the introduction fractures of both fracture set are cohesion-less with a friction angle of 30°. The pressure required for slip on both fracture sets is lower than the pressure required for hydraulic fracturing. However, in order to hydro-shear, the primary fracture set (shown in Figure 2) requires a lower pressure compared to secondary fracture set. A reservoir with a given fracture realization, but different values of fracture dilation angle is stimulated for 120 hours. Again, the DFN model used in this study has an exponent, α equal to 2, however the fracture size is capped to 300 m.

For each case, two different well positioning scenarios are considered. The stimulated fracture area and well positioning with models with different dilation angle are shown in Figure 13. The well positioning in the two cases are relatively similar, and it is intended to investigate the effect of slight variation in position of production wells. The strategy for well position is such that wells are located within the stimulated region, with a similar distance of approximately 500 m from the injection well. Also, wells are located on stimulated fractures with a minimum aperture more than 1×10^{-4} m. With the above three constraints, it was attempted to put the three well along primary, secondary fractures and in the middle location.

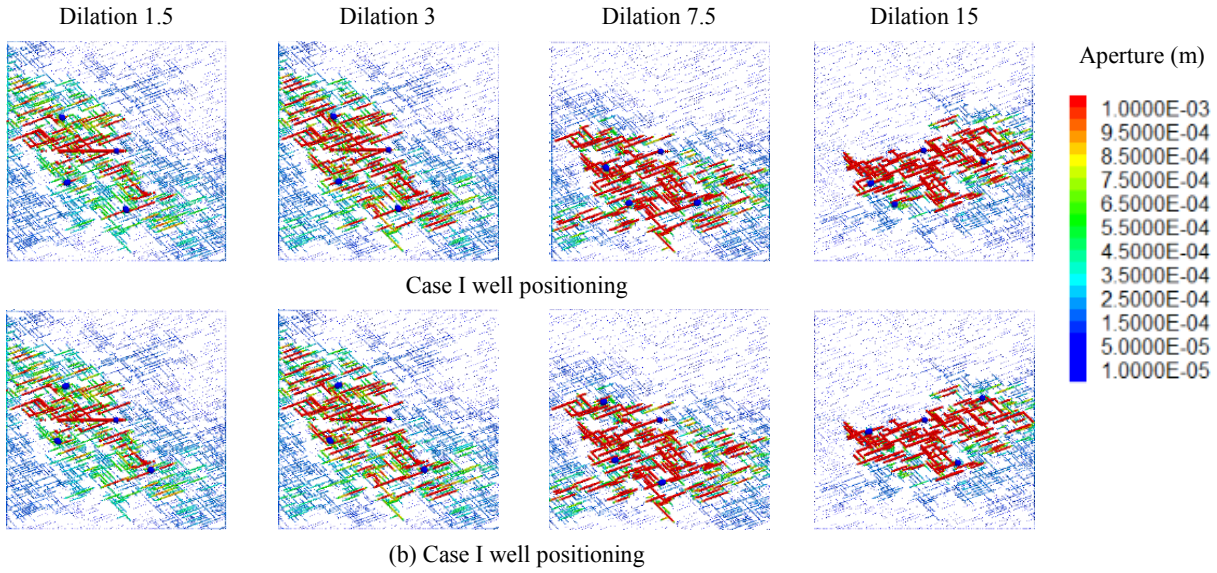

(b) Case I well positioning

Figure 13. Effect of fracture dilation angle: Contours of apertures in stimulated reservoir with different dilation angle, and location of injection and production wells

Figure 14 shows comparison of stimulation indices for these cases. The results of this study is in agreement with previous studies (Riahi and Damjanac, 2013a) and suggest the following.

- As dilation angle increases the average aperture of the stimulated region increases, thus it is expected that the stimulated area is better connected.
- As dilation angle increases the total stimulated area of fractures decrease (which is contributed to average higher aperture for stimulated fractures).
- As dilation angle increases the potential of hydraulic fracturing decreases. Figure 13 shows a clear path of hydraulic fracture for models with dilation angle of 1.5º and 3º.

Figure 15 shows the production indices for this study. These results show that in the case with no dilation angle, the recovered production rate was less than the rest of the case studies in which the production well produced all 100% of injected fluid. The

lower recovered rate resulted in lower generated power for the models with zero dilation angle. Except for this case, the rest of the models showed a monotonic response to variation of dilation angle. The overall response of models to variation of dilation angle is shown in Figure 16, and could be summarized as follows.

- For models with similar recovery rate, the temperature and generated power curves show similar trend to variation of dilation angle, in that higher dilation angle resulted in quicker temperature draw-down and lower generated power.
- The sensitivity of temperature and generated power to variation of dilation angle decreases as dilation angle increases, particularly for dilation angles above 3º as can be observed in Figure 15(a) and (b).
- The observed trend in injectivity is opposite to that of temperature and generated power. Higher dilation angles result in better injectivity, which is expected as higher dilation angle result in higher stimulated fracture aperture and better connectivity. Also, in contrast to the sensitivity of generated power, injectivity remains sensitive to values of dilation angle above 3 º.

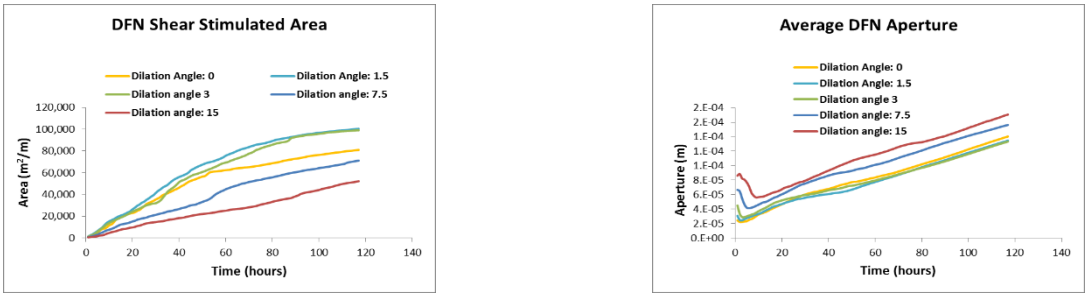

(a) (b)

Figure 14. Effect of fracture dilation angle: Stimulated indices.

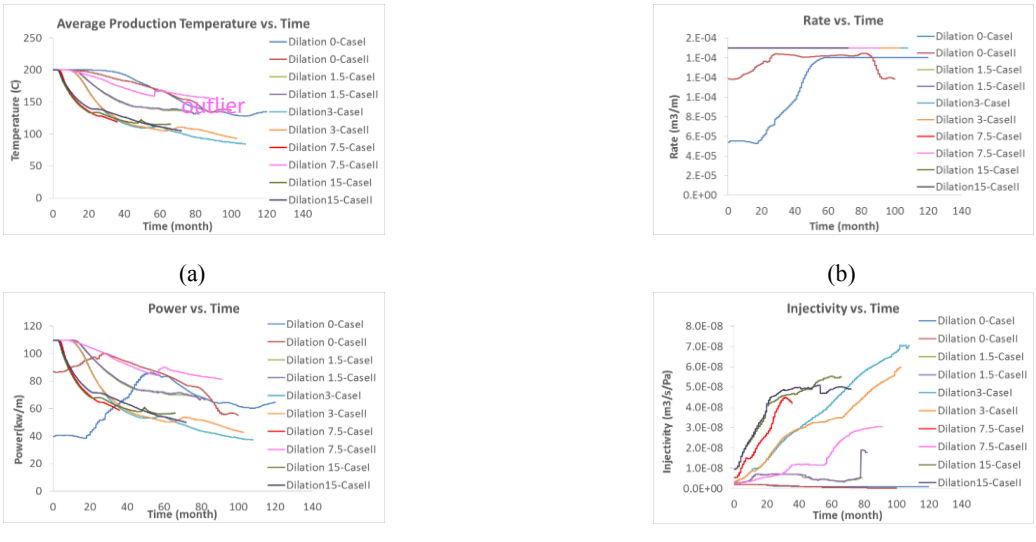

(a) (b)

(c) (d)

Figure 15. Effect of fracture dilation angle: Production indices.

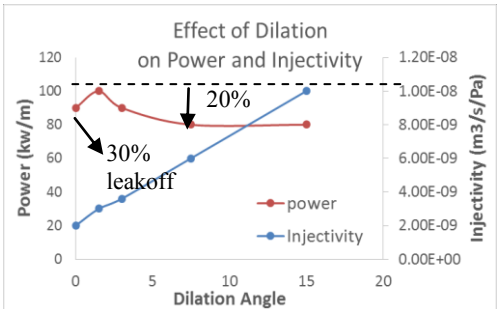

Figure 16. Graphs of average generated power (over five years of production) and injectivity (over first year) for different dilation angles.

2.5 Study 4: Effect of fracture length characteristics

This study focuses on effect of fracture length characteristics, in particular the exponent of fracture size distribution curve, (α in $n(l) \propto l^{-\alpha}$) on heat production. Effect of fracture length exponent on the stimulation indices is discussed in (Riahi and Damjanac, 2013 a, b, c). Figure 17 shows the DFN realizations used in this study. The ranking of 1-4 indicates the probability of having large fractures, with 4 being highest and 1 being the lowest.

Figure 18 shows that similar to the observation of previous studies, for similar injected volume shear stimulated area is directly correlated to the probability of having large fractures (at the size of the reservoir) in the model. Figure 19 shows contours of fracture apertures and indicate the stimulated fracture zone and the location of production wells chosen for this study. The distance between injection and production wells in all cases is approximately 750 m. Again the production wells are chosen such that they are within the stimulated region and also they fall directly on well stimulated fractures (with aperture of at least 1×10^{-4} m).

Figure 19 shows the stimulated fracture area and the location of production wells for two different scenarios. In Case I, for all models except for the model with exponent of 3, it was attempted to put the wells along primary fracture path. In the model with exponent 3 (Figure 19 (a)), however this scenario resulted in little recovery. Therefore, the position of well I was chosen based on the knowledge of flow path and fracture connectivity. Figure 19 shows the tortuosity of flow path in these models is correlated with the ranking in Figure 17, and is directly affected by probability of having large fractures in the model.

Effect of fracture exponent on production indices is shown in Figure 20. It can be observed from Figure 20(a) that for cases within recovery of 100%, the model with capped fracture resulted in slightly better generated power compared to model with exponent of 3, and both models showed better generated power comparted to model with exponent of 2.5. However, the difference is not very significant despite the more localized flow path in model with exponent of 2.5. The reason is contributed to the fact that in the model with exponent of 2.5 both wells are producing, while in the models with exponent of 2 and capped fracture size and 3, only one of the wells are producing.

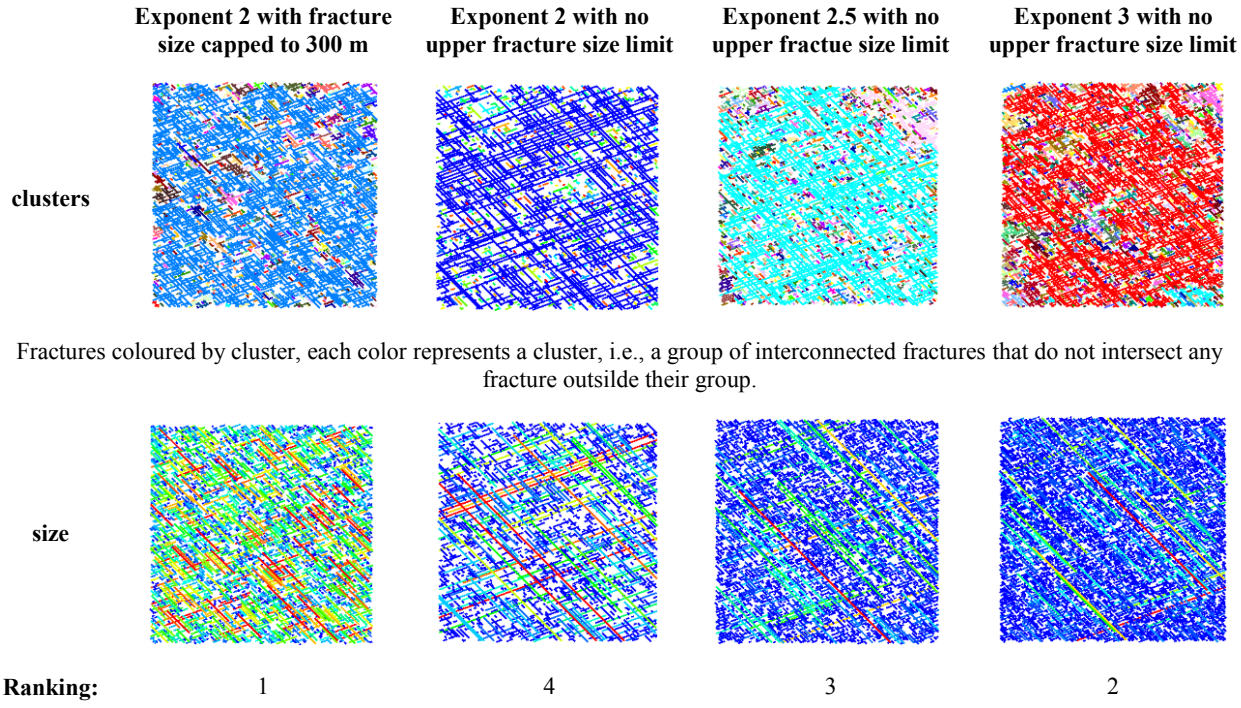

Fractures coloured by cluster, each color represents a cluster, i.e., a group of interconnected fractures that do not intersect any fracture outsilde their group.

Fractures colored by size: Red represents the largest fracture in the system, dark blue the smallest fractures

Figure 17. Fracture realizations for DFN models with different exponent and upper size fracture limit.

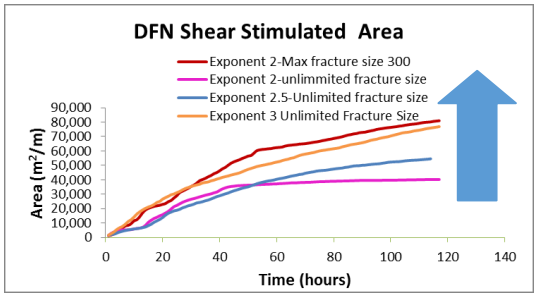

Decreasing probability of large fractures

Figure 18. Exponent of fracture size distribution: Shear stimulated area.

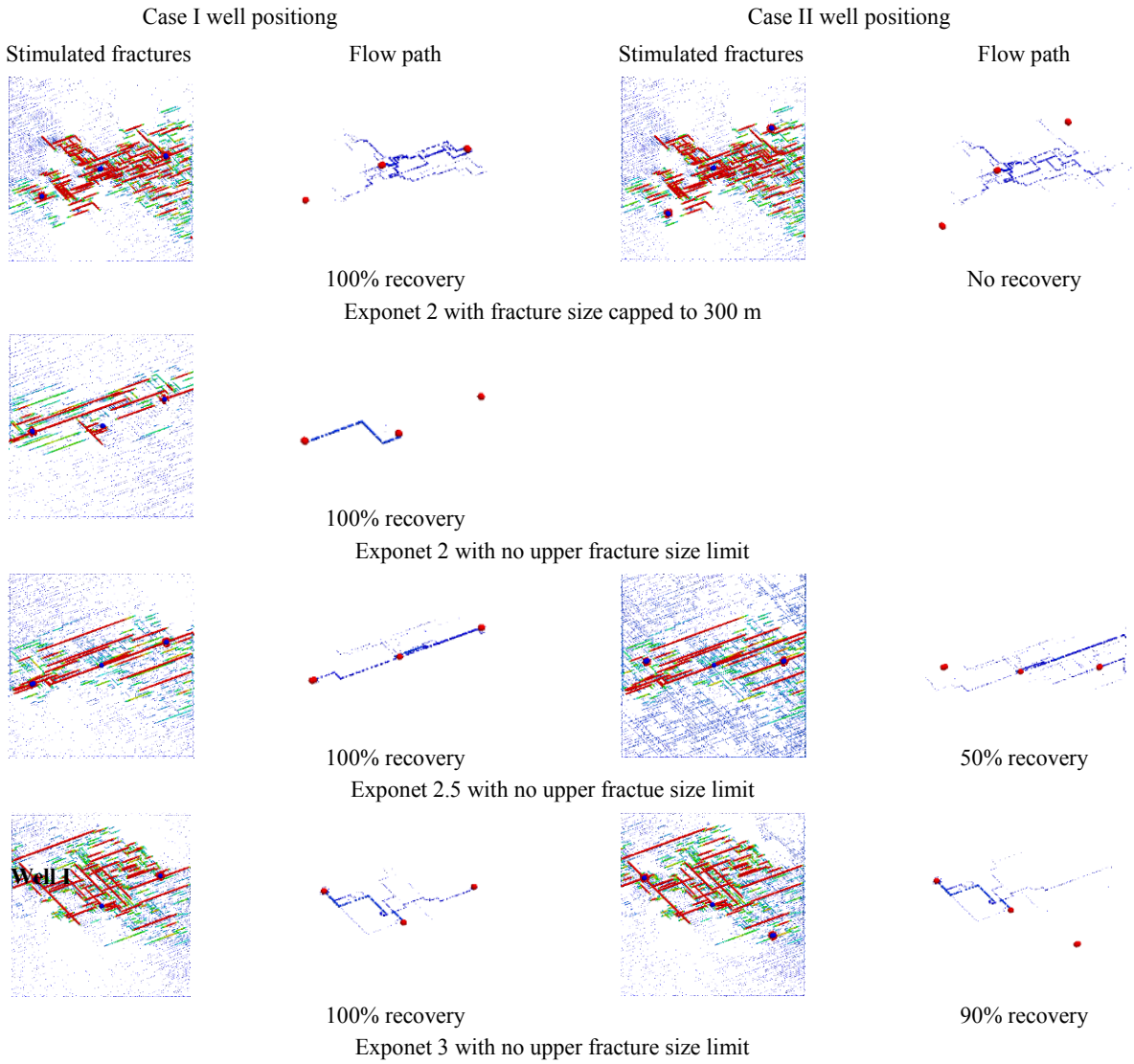

Figure 19. Exponent of fracture size distribution: Flow path and percentage recovery for DFNs with different fracture size exponent and position of the well (red color on stimulated fracture contours: fractures with aperture 1×10^{-3} m or higher).

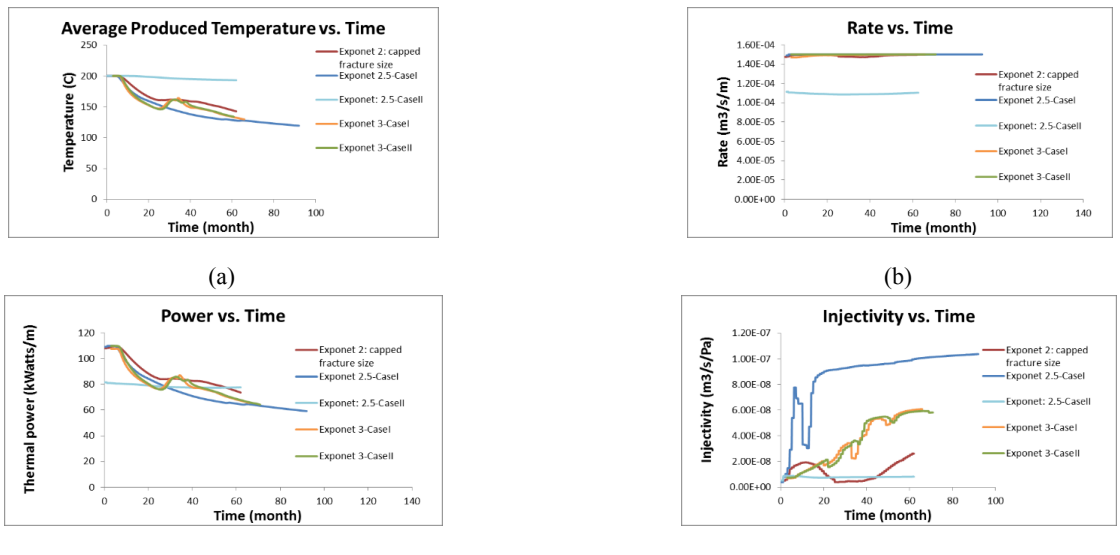

Figure 20. Exponent of fracture size distribution: Effect of production indices.

2.6 Study 5: Effect of production rate

The last case presented in this study focuses on the effect of production rate. For a stimulated reservoir with identical well positioning (shown in Figure 21), three different production rates are considered, 1×10^{-4} m3/s/m, 1.5×10^{-4} m^3/s/m and 1.9×10^{-4} m^3/s/m, which for an assumed thickness of 350 m, correspond to 30g kg/s, 52.5 kg/s, and 66.5 kg/s, respectively. The spacing between the injection and production wells is 750 m.

Figure 22 shows the effect of injection rate during production on the production indices. In these examples, the recovery is 100%, i.e., produced rate is equal to injection rate. As expected, when the production rate decreases, the generated power also decreases, however not with the same rate, due to slower draw-down in produced water temperature. In terms of injectivity, it seems for the considered stimulated models and the range of applied rate, higher rates result in better injectivity, again for the reason that pressure does not increase with the same rate that rate does. However, this observation can be affected by the relative permeability of the region around the injection well to applied rate. Finally, Figure 23 shows average produced power and injectivity for different production rates. For the given model and suggestion that a 50% increase in rate has resulted in a 20% increase in average generated power over the first five years.

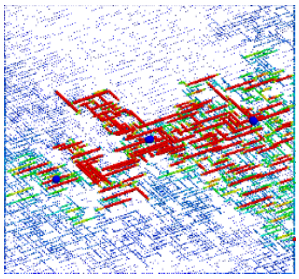

Figure 21. Effect of production rate: Stimulated volume and well positioning.

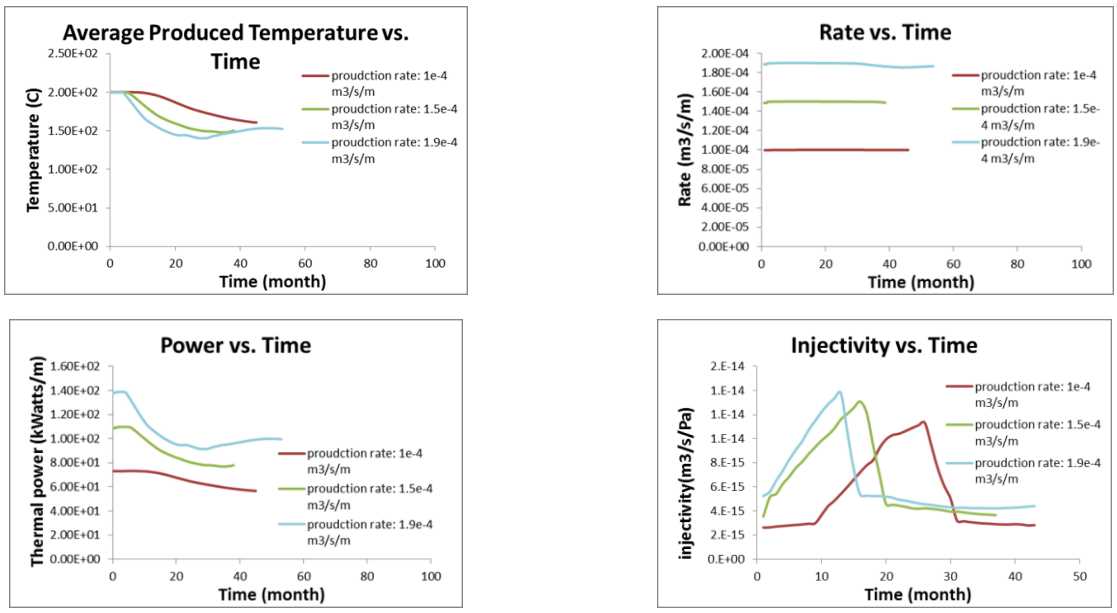

Figure 22. Effect of production rate: production indices.

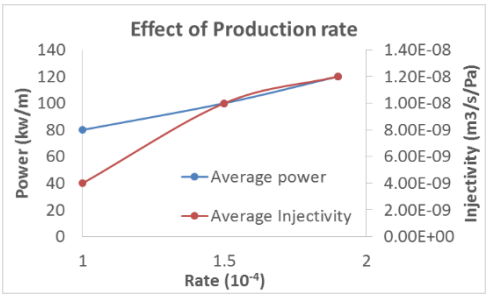

Figure 23. Effect of production rate: Average power and injectivity.

3. CONCLUSIONS

This paper presents the results of a series of sensitivity studies on thermo-hydromechanical response of EGS reservoir with respect to different field and operational parameters. A number of preliminary studies have been performed and reported in the past (Riahi and Damjanac, 2013 a, b, and c) and (Riahi et. al., 2014). In this paper, the effect of field parameters such as characteristics of the fracture network, dilation angle of fractures and operational parameters such as production rate were studied for more realistic conditions, i.e., longer periods of stimulation, larger reservoirs and wider spacing between injection and production wells (500 m to 800 m). Also, a systematic study with respect to effect of well position in terms of orientation of injection-production wells relative to fracture orientation, distance between injection-production well, and slight variation in positioning of the wells were performed. The conclusions of these studies can be summarized as follows.

1. While the effect of variation of different parameters on produced power, rate of temperature draw-down and injectivity can be quantitatively evaluated, their effect on recovery (or percentage of leak-off) cannot be qualitatively measured.

2. Recovery is greatly affected by the permeability of the region between injection-production wells relative to the rest of the reservoir. Therefore, it is critical that the position of the production well is chosen within the stimulated region and based on available knowledge of fracture characteristics, microseismic data and connectivity between injection and production wells. It is advisable that the region around the production well always be stimulated to guarantee injection and production wells fall in the same cluster of stimulated fractures, and to facilitate flow toward the production well.

3. In terms of well positioning, for similar produced rates, temperature draw down is mainly controlled by the length of flow path. A longer path results in slower temperature decay. Also, it seems that locating the production well directly along the primary fracture set relative to the injection well results in the least favorable condition for power generation. Therefore, as long as that the injection rate could be recovered, longer overall distance and more tortuous path (wells located off the primary fracture direction) are beneficial. However, injectivity is adversely affected by these conditions, i.e., longer distances and more tortuous paths can reduce injectivity by orders of magnitude.

4. As expected, increasing fracture spacing adversely affects produced power and injectivity. Overall, in the analyses performed that involved single-point injection, parallel flow within fractures were not observed. However, it seemed closer spaced fractures can lead to better dispersion of flow. It was observed that as fracture spacing increases, flow becomes more localized. In these cases, occurrence of a limited length hydraulic fracture helped in redistributing the flow to two oppositely located production wells.

5. Presence of dilation angle is critical for stimulation of EGS reservoirs. For similar injected volume during stimulation, higher dilation angle results in a smaller but better connected and more permeable stimulated volume. Although sensitivity of produced power to dilation angle above 3° reduces, injectivity remains sensitive to dilation angle, in that higher dilation angle results in better injectivity. Therefore, overall, higher dilation angle is preferable, although it must be noticed that in order to put wells at a desired distance, during stimulation higher volume of fluid needs to be injected into the reservoir compared to a case with lower dilation angle.

6. Fracture size characteristics affect probability of having large fractures (at the reservoir scale). Presence of small truncated fractures lead to more tortuous flow path and result in more disperse flow channels (although still localized), slower temperature draw down, and better produced power. As probability of long fractures (at reservoir scale) increases, the potential of flow localization also increases. If such faults or fractures happen to be within the path of flow, positioning the production well along these large fractures results in very good recovery, while positioning them off these fractures can lead to very slow recovery. In a more tortuous fracture network or networks with small truncated fractures, the chances of recovery when wells are off primary flow fractures are higher.

7. Finally, production rate affects both power and rate of temperature draw-down. However, the dependence is not linear. It is shown that an almost 50% reduction in production rate results in 20% reduction in power. This shows the effectiveness directing the flow to multiple well, and producing with lower rate from different locations.

REFERENCES

Gringarten, A.C., P.A. Witherspoon and Y. Ohnishi. Theory of Heat Extraction from Fractured Hot Dry Rock. Journal of Geophysics Research, v. 80 (8), March (1975).

Itasca UDEC (Universal Distinct Element Code), Version 5.0, Itasca Consulting Group, Inc., Minneapolis, (201)1.

Riahi A, and B. Damjanac, 2013a Numerical Study of Hydro-shearing in Geothermal Reservoirs with a Pre-existing Discrete Fracture Network, In proceedings, 38 Workshop on Geothermal Reservoir Engineering, Stanford University, SGP-TR-198, Stanford, California, February 11-13 (2013).

Riahi, A., and B. Damjanac. 2013b. Numerical study of interaction between hydraulic fracture and discrete fracture network. *Proceedings,* International Conference for Effective and Sustainable Hydraulic Fracturing Brisbane, Australia, May (2013).

Riahi, A., and B. Damjanac. 2013c. Numerical study of the interaction between injection and the discrete fracture network in enhanced geothermal reservoirs *Proceedings,* 47th U.S. Rock Mechanics/Geomechanics Symposium, San Francisco, June 20 (2013)

Riahi, A., Furtney, J. and Damjanac, B., Evaluation of Optimum Well Positioning in Enhanced Geothermal Reservoirs using Numerical Modeling, *Proceedings*, 38th Geothermal Resource council meeting, Portland, Oregon, (2014)